Statistical Models for Surface Renewal in Heat and Mass Transfer

Part III: Residence Times and Age Distributions at Wall Surface of a Fluidized Bed, Application of Spectral Density

L. B. KOPPEL, R. D. PATEL, and J. T. HOLMES

Argonne National Laboratory, Argonne, Illinois

A method was developed for estimating the age density of transporting elements at a transport surface by using the spectral density of the total element counts. Only total counts, and not individual element histories, need be observed. The method was compared with autocorrelation methods used in an earlier work. Residence times were measured for several sizes of particles at a particular wall surface of a stirred fluidized bed and at various gas velocities using both spectral density and autocorrelation methods. A dimensionless plot brought all data points near a single curve, valid only for this surface in this bed. Checks of these residence times against values obtained by direct observation of individual particles confirmed the methods.

The application of surface renewal models to transport problems requires a knowledge of the age distribution of transporting elements at the transporting surface. In an earlier paper, Koppel et al. (7) have developed equations relating the age distribution of elements to the time variation of the total number of tagged or tracer elements present at the transporting surface. The advantage of these methods is that laborious tracking of individual tagged elements is not required; only the total number of tagged elements present as a function of time is needed. This count of tagged particles with time will be referred to in the following as the *time series of particle counts*. The terms *elements* and *particles* will be used interchangeably, and, for convenience, tagged elements will be referred to simply as *elements*.

The objectives of the present work are to further develop the work of Koppel et al. (7) and to use these techniques to determine age distributions of particles at the surface of a fluidized bed. In particular, we develop the relationship between the age distribution and the spectral density of the time series of element counts. This is a logical step, since estimates of the spectral density possess better variance characteristics than do estimates of the autocovariance function (5). The autocovariance was related to the age distribution by Koppel et al. (7). Results from the two methods, spectral density and autocovariance, are compared for simulated series and for experimental particle counts observed at the wall surface of a fluidized bed. Additionally, relations are presented to estimate both the first and the second moments of the residence time distribution of particles. A knowledge of the second moment gives a measure of the spread of the residence time distribution and is also useful in calculating maximum and minimum transport coefficients as will be shown in a later paper (6).

Finally, we present data on mean residence times and the variances of the residence time distributions of particles at a wall surface in a gas-fluidized bed. These mean residence times are correlated in a dimensionless group with the ratio of gas velocity to velocity at minimum fluidization and will be used to predict experimental heat transfer coefficients in Part IV of this series (10).

L. B. Koppel is at Purdue University, Lafayette, Indiana. R. D. Patel is at Brooklyn Polytechnic Institute, Brooklyn, New York.

THEORY

Koppel et al. (7) have presented one method of estimating the age density $\phi(a)$ from the time series of tracer counts at the test surface, using autocovariances. The results of this section are based on the relations derived by these authors, the pertinent ones being stated below without proof.

The age density and residence time distribution functions are related by

$$\phi(a) = \frac{1 - F(a)}{\bar{\tau}} \tag{1}$$

where $\bar{\tau} = E\{\tau\}$, the mean residence time, $E\{\ \}$ being the expectation operator. From Equation (1) it may be seen that $\phi(a)$ is monotone decreasing.

The count $N(\tau)$ of elements at the surface at time τ is a Poisson distributed, stationary, random variable. Defining its autocovariance function $\psi(a)$ as

$$\psi(a) = E\{N\ (t + a)\ N(t)\} - \bar{N}^2 \tag{2}$$

we may show (7) that

$$\psi(a) = \frac{\bar{N}}{\bar{\tau}} \int_a^\infty (\tau - a)\ F(\tau)\ d\tau \tag{3}$$

AGE DENSITY FROM AUTOCOVARIANCES

This integral equation has the solution (7)

$$f(a) = \frac{\bar{\tau}}{\bar{N}} \frac{d^2\psi}{da^2} \tag{4}$$

or, by using Equation (1)

$$\phi(a) = \frac{-1}{\bar{N}} \frac{d\psi}{da} \tag{5}$$

The problem in using Equation (5) to estimate $\phi(a)$ is that $\psi(a)$ must be estimated from data. Taking derivatives of this estimate tends to magnify any errors. In general, the estimators for the autocovariance have complicated variance characteristics and often predict negative values beyond a certain value of a (7). This is, of course, incompatible with Equation (3). Thus, Equation (5) may be difficult to use in a practical situation. Estimation of $f(a)$ from Equation (4) is even more complex, since the second derivative of the estimator for $\psi(a)$ magnifies errors even further. Fortunately, for transport problems we are interested in $\phi(a)$ rather than $f(a)$.

Using Equation (5), Koppel et al. (7) further show that the mean residence time is given by

$$\bar{\tau} = -\frac{\bar{N}}{\left(\frac{d\psi}{da}\right)_{a=0}} \tag{6}$$

SPECTRAL ANALYSIS

In time series analysis, an approach via spectral analysis is often a fruitful alternative to the use of the autocovariance function. The motivation for using spectral analysis is threefold (5). [See also Blackman and Tukey (2).] First, the spectrum is particularly useful for frequency response studies. (The autocovariances may also be used for such studies, but the calculations are considerably more difficult.) Second, the sampling properties of spectra (or the variances of spectral estimates) are, in general, considerably simpler than those of the autocovariances (5). Third, when models are being constructed for a time series, spectral analysis frequently reveals important sources of fluctuations in the random process that would have otherwise been missed.

In this work, we are primarily interested in the simpler statistical properties of spectral estimates of the autocovariance function.

SPECTRAL DENSITY

Following Solodovnikov (11), the spectral density function $S(\omega)$, a function of the frequency ω, is defined as the Fourier transform of the autocorrelation function $R(a) = \frac{\psi(a)}{\psi(0)}$:

$$S(\omega) = 2\int_0^\infty R(a) \cos a\omega \, da \tag{7}$$

Equation (7) is the definition of $S(\omega)$ for a real, stationary time series with autocorrelation function $R(a)$.

RELATION BETWEEN THE SPECTRAL DENSITY AND THE AGE DENSITY

From Equation (3) and recalling that $\psi(0) = \text{Var}\{N\} = \bar{N}$, we obtain

$$R(a) = \frac{1}{\bar{\tau}} \int_a^\infty (\tau - a) \, f(\tau) \, d\tau \tag{8}$$

Using Equation (8) in (7) and reversing the order of integration, we get

$$S(\omega) = \frac{2}{\omega^2\bar{\tau}} \int_0^\infty f(a) \, (1 - \cos \omega a) \, da \tag{9}$$

Analogous to Equation (8), we have, using Equation (1)

$$R(a) = \int_a^\infty \phi(\tau) \, d\tau \tag{10}$$

which yields

$$S(\omega) = \frac{2}{\omega} \int_0^\infty \phi(a) \sin \omega a \, da \tag{11}$$

the analogue of Equation (9).

For example, for an exponential residence time density

$$f(\tau) = \frac{1}{\bar{\tau}} \exp(-\tau/\bar{\tau}) \qquad \tau \geq 0 \tag{12a}$$

$$= 0 \qquad \tau > 0$$

we obtain, using Equations (1), (10), and (11)

$$\phi(a) = \frac{1}{\bar{\tau}} \exp(-a/\bar{\tau}) \qquad a \geq 0 \tag{12b}$$

$$= 0 \qquad a < 0$$

$$R(a) = \exp(-a/\bar{\tau}) \qquad a \geq 0 \tag{12c}$$

$$S(\omega) = \frac{2\bar{\tau}}{1 + (\omega\bar{\tau})^2} \tag{12d}$$

Equations (9) and (11) are Volterra integral equations of the first kind in f and ϕ, respectively. They may be solved by using Fourier transforms to obtain (see Appendix*)

$$f(a) = \frac{2}{\pi} \int_0^\infty \left[1 - \frac{\omega^2\bar{\tau}S(\omega)}{2}\right] \cos \omega a \, da \qquad a \geq 0 \tag{13}$$

and

$$\phi(a) = \frac{1}{\pi} \int_0^\infty \omega S(\omega) \sin \omega a \, d\omega \qquad a > 0 \tag{14}$$

Note that Equation (14) is not valid for $a = 0$. However, we may obtain $\phi(0)$ from Equation (1) as $\phi(0) = 1/\bar{\tau}$. Independent methods for estimating $\bar{\tau}$ were presented in Part II (7).

Equation (14) appears to possess computational advantages over Equation (5). In Equation (5) a differentiation is necessary which tends to magnify errors. By using Equation (14), an integration is necessary which should tend to reduce errors. However, with both relations there is no guarantee that the estimated $\phi(a)$ will be positive for all positive a. Equation (14) possesses the disadvantage that it is not valid for $a = 0$. Values estimated near $a = 0$ will be in error because of this.

AVERAGE TRANSPORT COEFFICIENTS

In the usual case for studies of transport phenomena,

* Material has been deposited as document 00870 with the ASIS National Auxiliary Publications Service, c/o CCM Information Sciences, Inc., 22 W. 34th St., New York 10001 and may be obtained for $1.00 for microfiche or $3.00 for photocopies.

the age or residence time distributions are not of prime interest. Rather, one is interested in the average transport coefficient which is defined as an integral of the age distribution with the instantaneous coefficient

$$\overline{N}_{Nu} = \int_0^\infty N_{Nu}(a)\ \phi(a)\ da \tag{15}$$

Using Equation (14) in (15), we obtain

$$\overline{N}_{Nu} = \frac{1}{\pi}\int_0^\infty \int_0^\infty N_{Nu}(a)\ \omega S(\omega)\ \sin\ \omega a\ da\ d\omega \tag{16}$$

which is an alternative to the following relation presented by Koppel et al. (7):

$$\overline{N}_{Nu} = -\int_0^\infty \frac{dR}{da}\ N_{Nu}(a)\ da \tag{17}$$

Once again, the absence of a derivative in Equation (16) results in lower sensitivity to errors during actual computation. For the transport model $N_{Nu}(a) = 1/\sqrt{\pi a}$ (simple penetration theory), Equation (16) reduces to

$$\overline{N}_{Nu} = \frac{1}{\pi\sqrt{2}}\int_0^\infty \sqrt{\omega}\ S(\omega)\ d\omega \tag{18}$$

We thus have an expression for $\overline{N}_{Nu}$ in terms of the spectral density.

MOMENTS OF THE RESIDENCE TIME DENSITY

Higher moments of the residence time density function may be obtained by considering integrals of the form $\int_0^\infty a^n\ R(a)\ da$. Operating on Equation (3) in this manner and interchanging orders of integration, we obtain

$$\int_0^\infty a^n\ R(a)\ da = \frac{E\{\tau^{n+2}\}}{\overline{\tau}\ (n+1)\ (n+2)} \qquad n = 0, 1, 2, \ldots \tag{19}$$

In particular, setting $n = 0$ in Equation (19) and using Equation (7), we get

$$S(0) = E\{\tau^2\}/\overline{\tau} \tag{20}$$

Equation (20) presents a convenient method for estimating the variance of the residence time density once the spectral density is known.

ESTIMATORS

From experimental observation of the test surface we obtain the particle counts at discrete time intervals. We have $K + 1$ equally spaced observations of $N(t)$ at times $t_0 + j\Delta t$, $j = 0, 1, 2, \ldots, K$.

An estimator for $\overline{N}$ is constructed as

$$X_0 = \frac{1}{K+1}\sum_{j=0}^{K} N(t_0 + j\Delta t) \tag{21}$$

and for $\psi(j\Delta t)$ as

$$Y_j = \frac{1}{K+1-j}\sum_{i=0}^{K-j} (N_i - X_0)\,(N_{i+j} - X_0) \tag{22}$$

where $N_i = N(t_0 + i\Delta t)$.

Koppel et al. (7) have pointed out that X_0 is probably a better estimator for $\psi(0)$ than is Y_0. This is a consequence of the Poisson nature of the particle counts. As a consequence, better estimates of $\psi(j\Delta t)$ are expected from

$$Z_j = Y_j + X_0 - Y_0 \tag{23}$$

This forces $Z_0 = X_0$ as an estimate of $\psi(0)$. Tests on simulated series (which are discussed in detail below) showed that the estimates Z_j gave better results than did Y_j and so were used throughout.

Note that the continuous variable a in the theoretical expressions is replaced by the discrete variable $j\Delta t$ in the estimators. Derivatives must be approximated by differences. The variance of Y_j increases with j, since the sample size decreases, so that the estimates of the autocovariances are in greater error at higher $j\Delta t$.

Estimators for the spectral density of a real series with sample autocovariances Z_k are of the form (4)

$$S(\omega) = W(0)\Delta t + \frac{2}{Z_0}\sum_{k=1}^{n} W(k\Delta t)\ Z_k \cos\ (\omega k\Delta t)\ \Delta t \tag{24}$$

where $n = 0(K)$ but tends to infinity with K. Note that Equation (24) is a finite sum form of Equation (7), with a weight function $W(k\Delta t)$. For $W(k\Delta t)$ identically equal to 1, it can be shown (4, 12) that the variance of $S(\omega)$ does not converge to 0 as $K \to \infty$. In other words, $S(\omega)$ for $W(k\Delta t) = 1$ is not a consistent estimator. The value of n is generally chosen to be the lowest value for which Z_n approaches zero.

Various forms for $W(k\Delta t)$ have been proposed. In particular, the Bartlett estimator (4) uses

$$\begin{aligned} W(k\Delta t) &= 1 - \frac{k}{n} \qquad k \leq n \leq K \\ &= 0 \qquad\qquad k > n \end{aligned} \tag{25}$$

Other weight functions have been suggested (2). Computations on identical time series by using Equation (24) with Equation (25), and alternately with a Tukey estimator (2), did not give very different results in the present work. Equation (25) was, therefore, used throughout this work.

The asymptotic variance of the Bartlett estimator is (4)

$$\begin{aligned} \sigma^2[S(\omega)] &\approx \frac{2}{3}\ \frac{n}{K}\ S^2(\omega) \qquad \omega \neq 0 \\ &\approx \frac{4}{3}\ \frac{n}{K}\ S^2(0) \qquad \omega = 0 \end{aligned} \tag{26}$$

This estimator is biased (4). Furthermore, it is positive with probability one, a desirable feature since $S(\omega)$ is defined as always positive.

A problem arises when $S(\omega)$ is estimated from a series whose elements are separated by a finite time interval (which is the practical case). According to the sampling theorem of Shannon, estimates of $S(\omega)$ can be obtained only up to ω_N, the Nyquist frequency (5). This frequency is related to the shortest time interval separating two elements of the series, in this case Δt, by the expression

$$\omega_N = \frac{\pi}{\Delta t} \tag{27}$$

A second problem is aliasing, which has been discussed by Jenkins (5) and by Blackman (2). Aliasing occurs because estimates of the spectral density at a particular frequency ω are confounded with higher frequencies by fold back of these higher frequencies due to the sampling. This

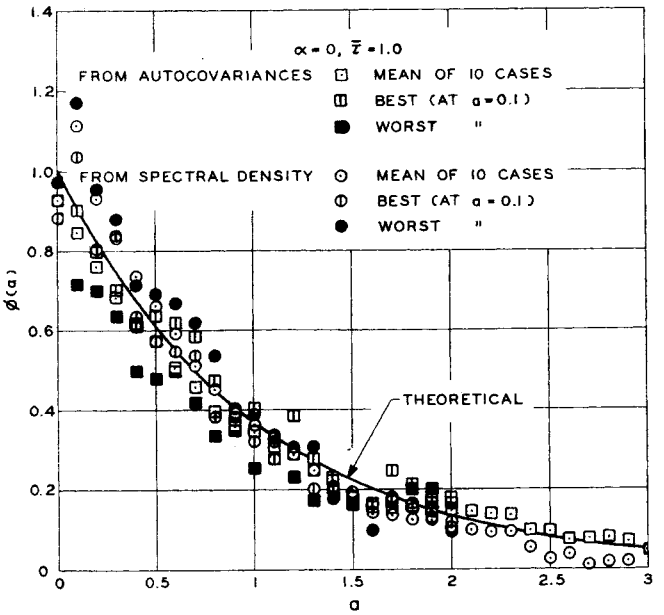

Fig. 1. Age density, theoretical and estimated, simulated series, $\alpha = 0$.

effect is reduced if $S(\omega)$ is small for $\omega > \omega_N$, that is, if one samples often enough.

The age density $\phi(a)$ can be estimated from the autocovariance estimators through Equations (5), (21), (22), and (23) as

$$\hat{\phi}_c(j\Delta t) = \frac{-1}{X_0} \frac{Z_j - Z_{j-1}}{\Delta t} \tag{28}$$

It can also be estimated from the spectral density estimators by using Equation (14) in truncated form:

$$\hat{\phi}_s(a) = \frac{1}{\pi} \int_0^{\omega_N} \omega \hat{S}(\omega) \sin \omega a \, d\omega \qquad a > 0$$

$$= \frac{1}{\hat{\bar{\tau}}} \qquad a = 0 \tag{29}$$

where $\hat{\bar{\tau}}$ is the estimate of the mean residence time derived from Equation (6) and given by

$$\hat{\bar{\tau}} = \frac{X_0 \Delta t}{Z_0 - Z_1} \tag{30}$$

The average transport coefficients can be estimated from the autocovariance estimators by using Equations (28) and (15):

$$\hat{\bar{N}}_{Nu} = \sum_{j=0}^{n} N_{Nu}(j\Delta t) \, \hat{\phi}_c(j\Delta t) \, \Delta t \tag{31}$$

From the spectral density estimators, we can estimate the average transport coefficients using Equation (24) in Equation (16) and using ω_N as the upper limit for ω in the integral in Equation (16):

$$\hat{\bar{N}}_{Nu} = \frac{1}{\pi} \int_0^{\omega_N} \int_0^{\infty} N_{Nu}(a) \, \omega \hat{S}(\omega) \sin \omega a \, da \, d\omega \tag{32}$$

For the simple penetration model $N_{Nu}(a) = 1/\sqrt{\pi a}$, this becomes, by using Equation (18)

$$\bar{N}_{Nu} = \frac{1}{\pi\sqrt{2}} \int_0^{\omega_N} \sqrt{\omega} \, \hat{S}(\omega) \, d\omega \tag{32a}$$

COMPUTATIONS

Problems arise when the integral in Equation (29) is evaluated numerically.

1. The integral is of a finite Fourier type. For larger values of a, the integrand exhibits a large number of positive and negative cycles, and numerical integration by conventional quadrature formulas results in accumulation of errors and loss of significance. One technique for numerical integration of such an integral is the Filon approximation (3). In this scheme, the function $\omega\hat{S}(\omega)$ is approximated by parabolic arcs over small intervals $\Delta\omega$. The integral is then computed as a finite summation. This scheme was used throughout.

2. When attempts were made to obtain $\phi_s(a)$ from Equation (29) by using actual values of $S(\omega)$ for a particular residence time distribution [for example Equations (12*b*) and (12*a*)], it was found that the values of $\hat{\phi}_s(a)$ oscillated about the true $\phi(a)$ at low values of a. This could occur because the equation is not valid for $a = 0$ and/or because the integral is truncated at the upper limit ω_N. It was found that the truncation actually caused the oscillations, because when the upper limit on the integral was increased sufficiently, the oscillations disappeared. The tail of the spectral density is thus important when $\phi(a)$ is estimated at low values of a. It is easy to see why this is so. An examination of Equation (28) shows that for small a, only a few cycles of the sine term are included in the integral, since ω_N is finite. This is what causes the oscillation, since theoretically an infinite number of cycles should be included. Hence for one value of a we obtain more negative cycles, while for a slightly different value of a we obtain more positive cycles, and so on, producing an oscillation in $\hat{\phi}_s(a)$. The effect diminishes as a increases, since now a large number of cycles of the sine term are included. The method adopted to overcome this problem is to extrapolate $\hat{S}(\omega)$ beyond ω_N by a negative

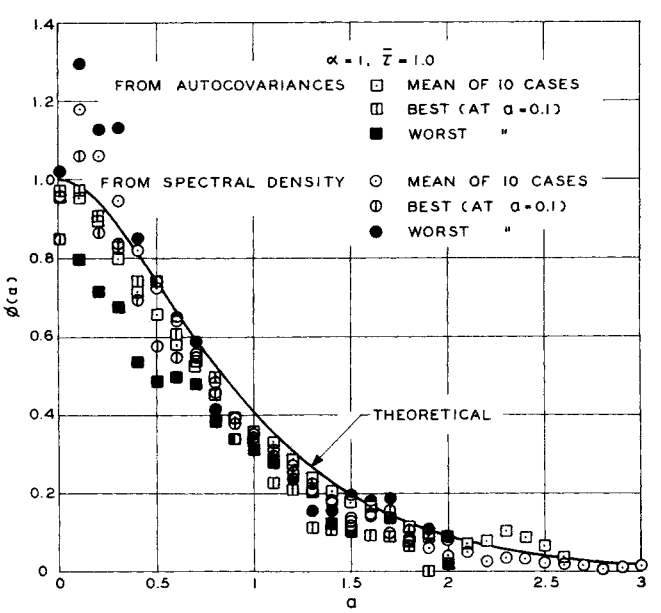

Fig. 2. Age density, theoretical and estimated, simulated series, $\alpha = 1$.

TABLE 1. RESULTS FROM SIMULATED SERIES

	$\alpha = 0$		$\alpha = 1$	
	Theor.	Sample*	Theor.	Sample*
Mean residence time	1	1.0104†	1	1.0049†
Second moment $E(\tau^2)$	2	2.0287†	3/2	1.5116†
$\overline{N}_{Nu}$ from autocovariances	1	0.9679†	1.061	1.0113
Ratio of std. dev. to $\overline{N}_{Nu}$ from autocovariances	—	0.078**	—	0.088**
$\overline{N}_{Nu}$ from spectral density	1	0.9610	1.061	0.9960
Ratio of std. dev. to $\overline{N}_{Nu}$ from spec. den.	—	0.038	—	0.036
$E(\tau^2)$ from spec. den.	2	1.733	3/2	1.573
Ratio of std. dev. to $E(\tau^2)$ from spec. den.	—	0.173**	—	0.234**

* From ten cases.
† Average of sample means of the ten cases.
** Standard deviation of 10 cases.

exponential. By definition, the area under the spectral density is π (*11*). This may be shown from Equation (7). The exponential tail is chosen to match the value of $S(\omega)$ at ω_N and to have an area such that the total area under $S(\omega)$ and the tail is π. Solodovnikov (*10*) points out that for monotone decreasing $R(a)$, $S(\omega)$ is also monotone decreasing. In the present situation, $R(a)$ is at least monotone decreasing (if not strictly decreasing), since counts at further removed times are less and less correlated with one another. Hence $S(\omega)$ is monotone decreasing. Thus, the choice of a negative exponential as the extrapolating function is consistent with the monotone decreasing characteristic of $S(\omega)$.

In tests to check the method, theoretical values [for example, from Equation (12*d*)] of $S(\omega)$ were used for $\omega \leq \omega_N$ and the exponential tail used beyond ω_N. The values of $\phi_s(a)$ thus obtained exhibited no oscillations and were in agreement with the theoretical values of $\phi(a)$, which for the above example are given by Equation (12*b*).

When an actual series is being analyzed, the estimator for the spectral density [Equation (24)] is such that the area from $\omega = 0$ to ω_N under $\hat{S}(\omega)$ is very near π. Consequently, the required area under the exponential tail must be estimated by considering what the area under $S(\omega)$ should be beyond ω_N for typical residence time distributions. It may be shown (see Appendix*) that for residence time densities of widely differing form (an exponential and a pulse), the area under $S(\omega)$ beyond the Nyquist frequency is $2\Delta t/\pi\overline{\tau}$, to second-order accuracy. This value is therefore chosen as the area of the exponential tail.

In summary, when we use Equation (29), a Filon approximation is used to evaluate the integral and a correction is applied to $\hat{\phi}_s(a)$ as

$$\hat{\phi}_s(a) = \frac{1}{\pi}\int_0^{\omega_N} \omega \hat{S}(\omega) \sin \omega a \, d\omega + \frac{1}{\pi}\int_{\omega_N}^{\infty} \omega c_1 \exp(-c_2\omega) \sin \omega a \, d\omega \quad (33)$$

where c_1 and c_2 are constants evaluated by matching the exponential tail to the value of $\hat{S}$ at ω_N and by fixing its area from ω_N to ∞ at $2\Delta t/\pi\overline{\tau}$.

VERIFICATION AND RESULTS

The methods developed above were tested in two ways. First, the equations were used on time series of particle counts of known residence time density generated by a Monte Carlo technique. This provided a convenient means of checking the accuracy of the estimators described above, since the estimates could be compared with the known theoretical values. Second, the methods were applied to time series of particle counts observed at the wall of a fluidized bed. The sample age density for some of these series was also obtained by direct particle tracking. Thus, a comparison could be made between the directly measured sample age density and that estimated from the autocovariances and spectral density of the time series of particle counts at the surface.

COMPUTER SIMULATION

The equations developed above were tested for a simulated time series generated on a computer by a Monte Carlo technique (*7*). The time series of particle counts was generated for a known residence time distribution of the gamma form. For such a distribution, the theoretical age density, autocovariance function, and spectral density were known through Equations (1), (3), and (9). [See Koppel et al. (*7*).] The simulated series was used to estimate the quantities in Equations (28) to (32) developed above, and a comparison was made between the estimates and the theoretical values. It must be kept in mind that each simulated series had an inherent sampling variance (by virtue of the fact that the Monte Carlo technique samples the true residence time density to generate the series of particle counts) which biased any results based on it. Several statistically independent series were therefore generated with the same theoretical residence time distribution, and the sample means and variances of the estimated age densities, etc., were computed before comparison was made with the theory.

Simulated series were generated for two forms of the gamma residence time distribution by using $\alpha = 0$ and $\alpha = 1$ (*7*). Ten independent series were generated for each α value. Other parameters were chosen as $\overline{\tau} = 1.0$, $\Delta t = 0.1$, $\overline{N} = 20$, and $K + 1 = 1{,}500$.

AGE DISTRIBUTION

Figures 1 and 2 show the theoretical age distribution for the two α values compared with values estimated by the autocovariance method [Equation (28)] and by the spectral density method [Equation (33)]. The means

TABLE 2. PROPERTIES OF FLUIDIZED PARTICLES

Particle type	Shape	Wt. mean particle diam., ft. $\times 10^3$	Density, lb./cu. ft.	Min. fluidized vel. (superficial), ft./min.
Cellulose acetate	Spherical	10.5	81.2	199.8
No. 1 glass	Spherical	2.65	154	83.5
No. 2 glass	Spherical	1.94	154	50.8
No. 3 glass	Spherical	1.03	154	19.0

* See footnote on p. 457.

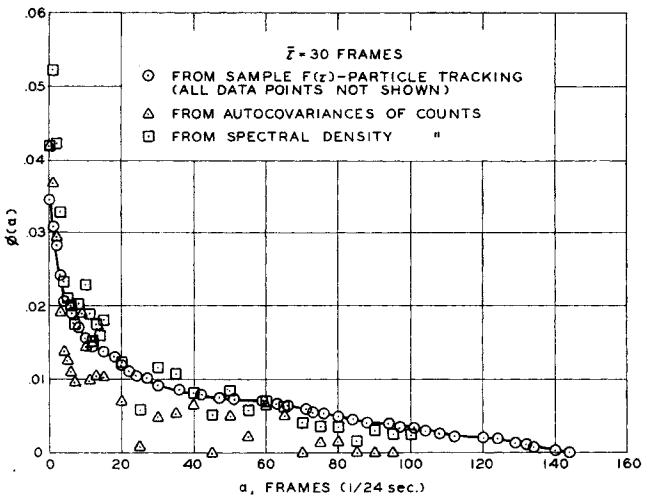

Fig. 3. Age density at fluidized bed wall, sample and estimated, run 1, No. 1 glass.

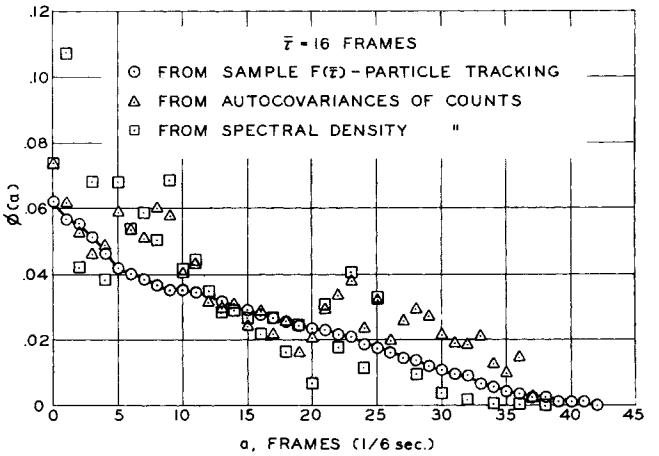

Fig. 4. Age density at fluidized bed wall, sample and estimated, run 2, cellulose acetate.

from the ten cases along with the worst and best cases are plotted for each method. The worst and best cases were arbitrarily chosen as the cases for which $\phi(a)$ had the greatest and least deviation, respectively, at $a = 0.1$.

The results on these figures show that for the parameters chosen, reasonably accurate estimates of $\phi(a)$ may be obtained by using either the autocovariance or spectral density methods. No direct quantitative comparison between the two estimates of $\phi(a)$ was made because one must assign an arbitrary single numerical value (similar to a performance criterion in optimization theory) to describe the agreement between $\hat{\phi}(a)$ at each a and the theoretical curve, and the result of the comparison will depend on the criterion chosen, and because the age density is not normally a quantity of primary interest but is an intermediate quantity used to compute average transport coefficients. For these reasons, the methods were compared on their estimates of the average transport coefficient.

AVERAGE COEFFICIENTS

Average coefficients were found for the model $N_{Nu}(a) = 1/\sqrt{\pi a}$ by using Equations (31) and (32a). The mean and variance of the ten cases for each α value are shown in Table 1. The summation in Equation (31) was truncated at $n\Delta t = 5.0$; beyond this value the autocovariances are essentially zero. The means of the ten estimates of $\overline{N}_{Nu}$ for both α values are within 5% of the theoretical value, whatever method is used. Note, however, that the internal scatter in the results from the spectral method is approximately half that from the autocovariance method. In any one case, therefore, the spectral method will probably give a more accurate value of the average transport coefficient for the chosen values of the parameters.

As an example of the effects of the reduced scatter achieved with the spectral density estimate, suppose we are trying to compare $\overline{N}_{Nu}$ for the two α values. In other words, two experiments have been run, and, unknown to the experimenter, the shape of the age density has changed through the parameter α. Theoretically then, a change of 1.061 to 1.000 = 0.061 should be observed in $\overline{N}_{Nu}$. By using the autocovariance, the estimated difference is 0.043 with a standard error of 0.037, while use of the spectral density gives an estimated difference of 0.035 with a standard error of 0.0166. Therefore, with the spectral density estimate the observed difference is significant at a confidence level of 95% (by using a t test with 18 deg. of freedom), while with the autocovariance estimates we would be more reluctant to conclude that a difference exists, since the significance level is less than 80%.

The autocovariance and spectral density methods should be considered complementary rather than competitive. The above results show that there is an advantage to applying both methods and to basing conclusions on the joint estimates, thus hopefully taking advantage of their respective strengths and diluting the effects of their respective weaknesses.

SECOND MOMENTS OF THE RESIDENCE TIME DENSITY

Second moments were computed for the various cases for the two alpha values by using Equation (20). The sample means and standard deviations for the ten cases for each alpha value ($\alpha = 0$ and $\alpha = 1$) are shown in Table 1. It may be seen that the mean of the ten cases is fairly close to the theoretical value for each value of alpha. For $\alpha = 0$, the deviation is about 15% and for $\alpha = 1$ about 5%. The standard error about the mean is about 20% for both cases. We thus have a reasonable estimate of the variance of the residence time distribution, which gives us more information about its shape. Note that this is obtained solely from information on total particle counts at the surface.

AGE DENSITIES AT WALL SURFACE OF A FLUIDIZED BED

The mean residence times and age distributions of particles at a section of the wall of a gas fluidized bed were experimentally measured, and the results are discussed in this section. A full description of the experimental apparatus and technique has been given by Patel (8). The equipment is similar to that used by Koppel et al. (7), with some modifications. Only a brief outline will be given here.

The fluidized bed column consisted of a 4-in. I.D. stainless steel pipe with a 2½ in. wide flat Lucite plate mounted as a chord along the entire column length in a slot cut in the pipe. The flat surface eliminated distortion when the wall was photographed. Four types of particles were used, three different sizes of glass and one of cellulose acetate. Their properties are given in Table 2. A few white particles among the otherwise identical black particles served as tagged elements. Air was used as the fluidizing medium throughout.

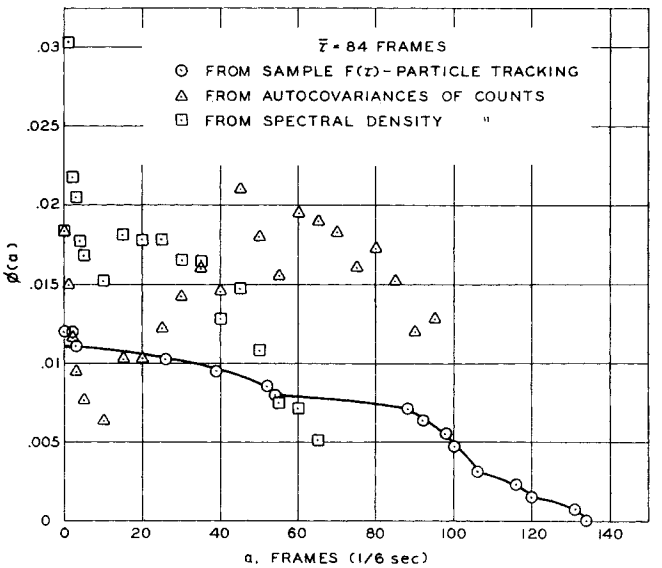

Fig. 5. Age density at fluidized bed wall, sample and estimated, run 3, cellulose acetate.

With the bed filled to a depth of about 8 in. and fluidized, a 2 in. high by 1½ in. wide section of the Lucite plate, centrally located and approximately 5 in. above the distributor plate, was photographed by a synchronously driven Arriflex 35 mm. motion picture camera operating at a constant 24 frames/sec. Bubbles were eliminated by stirring the bed just below the test surface with a paddle type of stirrer at about 400 rev./min. (The runs with acetate used approximately 300 rev./min.) The stirrer broke up the bubbles before they reached the test surface. The absence of bubbles was desired for later application of the residence time measurements to heat transfer studies, to be presented in Part IV (*10*).

The film record was analyzed to obtain the time series of counts of tracer particles at the test surface. These counts were used to obtain the average residence times by Equation (30) and the age distributions by using the autocovariance and the spectral techniques.

For three of the nineteen runs, two with the acetate particles and one with No. 1 glass, individual particle tracking was also done. Details of the method have been given by Koppel et al. (*7*) and by Patel (*8*). Briefly, it entails following each tagged particle so that its entrance and exit times, and hence its residence time, are known. The cumulative distribution of residence times $F(\tau)$ and the sample mean residence time are computed from the residence times of all the particles tracked. This yields $\phi(a)$ through Equation (1). The results from particle tracking and from the counts methods can then be compared. Table 3* summarizes the experimental conditions and results for these three runs. Figures 3 to 5 show the age distributions for these runs.

Figure 3 shows the estimate of $\phi(a)$ obtained by particle tracking (the sample age density) and that predicted by the autocovariance and spectral methods, for the run with No. 1 glass. For this run, relatively many particles (181) were involved. As a consequence, we obtain better estimates of $\phi(a)$. The predicted age density lies fairly close to the sample age density for both methods, except for large values of a which are usually unimportant in computing $\overline{N}_{Nu}$.

Figure 4 shows the sample $\phi(a)$ and the values estimated by the two methods for the first run with cellulose acetate. The scatter is considerably greater. One reason is that significantly fewer particles (102 vs. 181) were involved, leading to higher sampling variances. Figure 5 shows the results for the second run with cellulose acetate. Only fifteen particles were involved in this run, and this is probably the reason for the extensive scatter between estimated values and the sample $\phi(a)$.

The moments of the residence time density obtained by the various methods for these three runs are compared in Table 3.* The variance is defined in dimensional quantities as

$$\sigma^2 = E\{\theta^2\} - E^2\{\theta\}$$

In the counts method, the ratio $E\{\theta^2\}/E\{\theta\}$ is estimated by using $S(0)$, as in Equation (20). $E\{\theta\}$ is obtained as in Equation (30). For particle tracking, if θ_i is the observed residence time of the i^{th} tracer particle, the estimates presented are obtained from

$$\overline{\theta} = \frac{1}{N}\sum_{i=1}^{N} \theta_i$$

$$\hat{\sigma}^2 = \frac{1}{N-1}\sum_{i=1}^{N} (\theta_i - \overline{\theta})^2$$

For run 1, the agreement between moments obtained by the two methods is quite good (within 17% on $\overline{\theta}$ and 20% on $\hat{\sigma}$), probably because of the larger number of particles tracked giving better sampling statistics. The agreement becomes successively worse from run 1 to run 2 to run 3 because of fewer samples. For run 3, the agreement is poor, but note that only fifteen particles were involved.

The results obtained for these three test runs lead to two conclusions. First, in applying the total counts methods one must be careful to ensure that a reasonable number of particles is involved. This can be done without individual particle tracking by using the observed changes method for estimating the average entrance rate r from total counts, as presented earlier in Part II. Multiplication of r by the total number of frames gives an estimate of the number of particles involved. For all runs performed here with glass particles, this number was comparable to or greater than that obtained in run 1, and therefore we do not expect serious error from this cause. Second, although considerable scatter may occur in either the autocovariance or spectral density estimates of $\phi(a)$, the estimates of the mean residence time and standard deviation are acceptably accurate, provided sufficient particles are involved. In Part V, the estimate of the mean, θ and of the ratio of standard deviation to mean will be used to establish narrow upper and lower bounds on $\overline{N}_{Nu}$ without any further knowledge of $\phi(a)$.

AVERAGE RESIDENCE TIMES AT THE WALL OF THE FLUIDIZED BED

Average residence times and ratios of standard deviation to mean were found experimentally at different gas velocities for the three sizes of glass particles and for the cellulose acetate particles. (See Table 2 for properties.) These quantities were estimated from the time series of total tracer particle counts at the surface by using the methods presented above.

* See footnote on p. 457.

* See footnote on column 1.

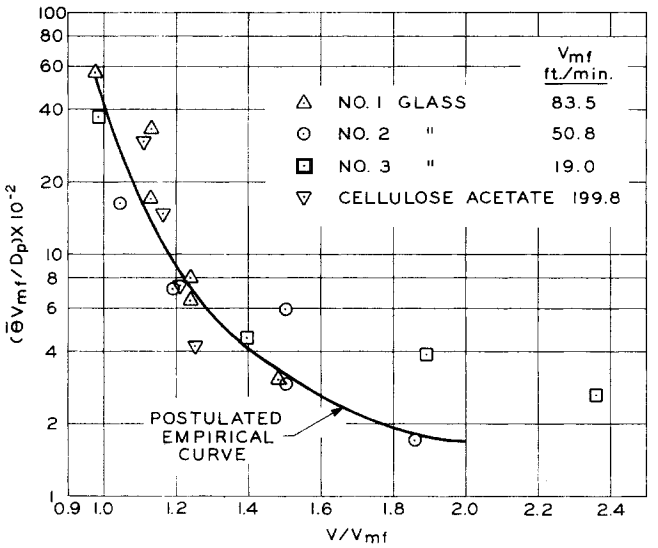

Fig. 6. Relation between dimensionless particle residence time at fluidized bed wall and gas velocity ratio.

The residence times of the particles at the wall are affected by particle properties such as the diameter, density, and shape, as well as by the superficial gas velocity v. The minimum fluidization velocity v_{mf} is a good characterization of the shape and density of the particles. Also, the residence times should be shorter for higher gas velocities. A universal relation between the average residence times and the gas velocity may therefore be postulated to be of the dimensionless form $\overline{\theta}\, v_{mf}/D_p$ vs. v/v_{mf}.

The data for the glass and cellulose acetate particles are plotted in such a form in Figure 6. Note that these data are for a specific, bubble free surface. The data points lie close to a single curve and show a definite trend, partially substantiating the postulated relation. An empirical curve has been drawn through the data for estimating residence times for other particle systems. The two data points for No. 3 glass at high v/v_{mf} are probably higher than they should be. This is due to the observed buildup of an electrostatic charge on these smallest particles. Although an antistatic spray and humidified air were used to reduce static, some slight effects were observed for the smallest particles. The presence of the charge causes the residence times to be high. Static effects were not observed for the larger No. 1 and No. 2 particles.

Note that the empirical curve can be used only for the particular geometry of this investigation. Certainly, the speed of stirring of the bed, the height of the transporting surface, and its elevation above the distributor, etc., would affect the numerical values of $\overline{\theta}$. What has been postulated is a unique relation between $\overline{\theta}\, v_{mf}/D_p$ and v/v_{mf} for a particular geometry. There is some question as to whether the effect of particle density is adequately included through v_{mf}, or whether there is a direct dependence on another dimensionless parameter containing particle density. The present data cannot resolve this question, as the density was not adequately varied. The cellulose acetate particles are of a somewhat different density from the glass, but not sufficiently so as to warrant any conclusions on this question from these data.

SECOND MOMENTS OF THE RESIDENCE TIME DISTRIBUTION

The second moments of the residence time distribution were estimated from Equation (20). These are plotted in Figure 7 as the ratio $\beta = \sigma\{\tau\}/\overline{\tau}$ [this is identical to

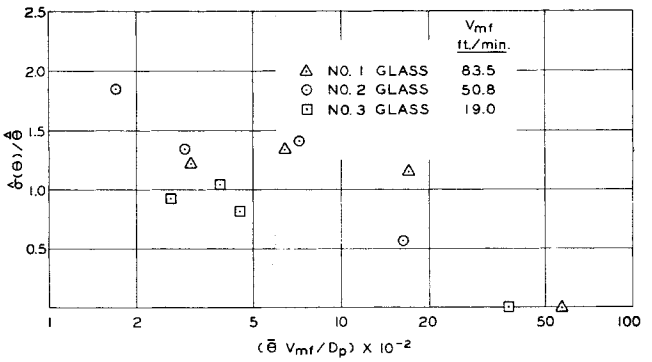

Fig. 7. Ratio of standard deviation of residence times to the average residence time plotted against the residence time group $\overline{\theta} v_{mf}/D_p$.

$\sigma\{\theta\}/\overline{\theta}$] vs. $\overline{\theta}\, v_{mf}/D_p$. There is considerable scatter, and no firm correlation can be established. However, it appears that β tends to decrease as $\overline{\theta}$ increases. In particular, the standard deviation is very small for long average residence times (low gas velocities) for all three glass sizes. In other words, the distribution is concentrated near the mean. For very short residence times (higher gas velocities), the standard deviation is almost twice the mean residence time, implying a widely spread distribution of residence times. This fact has significance when minimum and maximum possible coefficients for a particular $\overline{\tau}$ are considered in Part V (*6*). Also, if arbitrarily an exponential residence time distribution with the observed mean residence time is used to calculate average transport coefficients from a given instantaneous coefficient, the predicted coefficients should be low for the long residence times and may be high for the short residence times. This has an implication in Part IV of this series (*10*), when average heat transfer coefficients are predicted.

CONCLUSIONS

Reasonable estimates of the age density of particles at a transporting surface can be made from observations of only the total tracer particle count with time. Both the autocovariance and the spectral methods may be used for this purpose.

The average transport coefficient and the mean and variance of the residence time density may also be estimated with acceptable accuracy from the time series of tracer particle counts. In the present study, the spectral method estimated the average transport coefficient with a lower standard error.

In the tests on a fluidized bed system, both the autocovariance method and the spectral density method gave acceptable estimates of the age density, average transport coefficient, and the mean and variance of the residence time distribution.

The experimental data on average residence times, of particles at a specific surface on the wall of the particular fluidized bed used in this study, correlate satisfactorily as $\overline{\theta}\, v_{mf}/D_p$ vs. v/v_{mf}. A possible additional effect of particle density should be sought in future work.

The spread in the residence time distribution of particles at this particular surface of this fluidized bed is apparently greater for short residence times (high gas velocities); for long residence times (low gas velocities) the distribution is more concentrated near the mean.

ACKNOWLEDGMENT

Work was performed under the auspices of the U.S. Atomic

Energy Commission through Contract No. W-31-109-Eng-38.

NOTATION

a = dimensionless age, random variable
D_p = particle diameter
$E\{\ \}$ = expected value
f = residence time density function
F = residence time distribution function
$F\{\ \}$ = Fourier transform
$K+1$ = number of equally spaced observations
n = lowest number for which $Z_n \rightarrow 0$
N = total number of particles observed
N_{Nu} = transport coefficient
$\overline{N}_{Nu}$ = average transport coefficient
$N_{Nu}(a)$ = instantaneous transport coefficient
$N(t)$ = number of elements in residence at time t, random function
P_N = probability mass function
R = autocorrelation function
S = spectral density function
t = time
v = superficial gas velocity
v_{mf} = superficial gas velocity at minimum fluidization
W = weighting function
$W(j\Delta t)$ = weight function in estimator for spectral density
X_0 = estimator for $\overline{N}$
Y_j = estimator for $\psi(j\Delta t)$
Z_j = modified estimator for $\psi(j\Delta t)$

Greek Letters

α = shape factor for gamma distribution
Δt = time difference between observations
θ = dimensional residence time
$\overline{\theta}$ = $E\{\theta\}$
$\sigma\{\ \}$ = standard deviation
$\sigma^2\{\ \}$ = variance
τ = dimensionless residence time, random variance
$\overline{\tau}$ = $E\{\tau\}$
ϕ = age density function
ψ = autocovariance function
ω = frequency
ω_N = Nyquist frequency

Superscripts

$-$ = mean value over distribution
$\wedge$ = estimate

LITERATURE CITED

1. Abramowitz, M., and I. A. Stegun, "Handbook of Mathematical Functions with Formulas, Graphs, and Mathematical Tables," Natl. Bur. Stds., App. Math. Ser. 55, 4th printing (Dec., 1965).
2. Blackman, R. B., and J. W. Tukey, "The Measurement of Power Spectra from the Point of View of Communication Engineering," Dover, New York (1958).
3. Davis, P. J., and R. Rabinowitz, "Numerical Integration," Blaidsell, Mass. (1967).
4. Grenander, U., and M. Rosenblatt, "Statistical Analysis of Stationary Time Series," Wiley, New York (1957).
5. Jenkins, G. M., *Technometrics*, 3, No. 2, 133-166 (1961).
6. Koppel, L. B., "Statistical Models for Surface Renewal in Heat and Mass Transfer: Part V, Maximum and Minimum Transport Coefficients."
7. ———, R. D. Patel, and J. T. Holmes, *AIChE J.*, **12**, 947-955 (1966).
8. Patel, R. D., Ph.D. thesis, Purdue Univ., Lafayette, Ind. (1967).
9. ———, *ANL-7353*, Argonne National Laboratory, Argonne, Ill.
10. ———, L. B. Koppel, and J. T. Holmes, *AIChE J.*
11. Solodovnikov, V. V., "Introduction to the Statistical Dynamics of Automatic Control Systems," Dover, New York (1960).
12. Wilks, S. S., "Mathematical Statistics," Wiley, New York (1962).

Part IV: Wall to Fluidized Bed Heat Transfer Coefficients

Heat transfer coefficients were measured for glass particles at the same wall surface of a fluidized bed for which glass particle residence times were measured in a previous study. The data compared well with theoretical predictions of the dependence of heat transfer coefficients on particle residence times. Heat transfer coefficients for metal particle systems, for which direct measurements of residence times were not available, were predicted with fair accuracy by estimating residence times from a dimensionless correlation proposed in a previous study. The ability of the particle surface renewal models to accurately predict heat transfer coefficients is strong evidence of their physical validity.

DISCUSSION OF PREVIOUS WORK

Current information strongly suggests that heat transfer from a surface to a gas fluidized bed is a surface renewal transport process. Several authors have proposed surface renewal models for predicting wall to fluidized bed heat transfer coefficients. Mickley and Fairbanks (*9*) envisage clumps of particles, or packets, arriving at the heated surface, receiving heat by unsteady state transfer, and returning to the bulk of the bed. The packets have the properties of the bed at minimum fluidization conditions. The heat transfer coefficient is shown to be proportional to a stirring factor and to the square root of the packet thermal conductivity, specific heat, and density. The stirring factor depends on the frequency of renewal of the packets at the heated surface and is assumed to include the effect of particle diameter. The deficiencies in this model are that the heat transfer coefficient is directly proportional to the square root of particle heat capacity, which is unrealistic, as pointed out by Ziegler et al. (*15*); and the predicted heat transfer coefficient is inversely proportional to the square root of the mean age of the packets, so that at zero age the predicted coefficient is infinite, whereas at infinite age (corresponding to minimum fluidization conditions) it is zero.

Baskakov (*2*) proposed a similar model with an added contact resistance to heat transfer located at the wall-facing surfaces of the particles which are in contact with the wall. Because of the contact resistance, the heat transfer coefficient for zero age does not become infinite but is determined by the finite contact resistance at the wall. However, for infinitely large values of the age, the coefficient goes to zero, which is a theoretical deficiency.

Ziegler, Koppel, and Brazelton (*15*) have proposed a